# Supporting Information for

## Quantitative Connection between Macroscopic Stress and Bond-Breaking Force Enabled by Time-Stamped Mechanochemical Fluorescence

Zeyu Wang,[1] Devavrat Sathe,[1] Ming-Chi Wang,[1] Junfeng Zhou,[1] Zichen Ling,[2] Qixin Zhou,[2]* Junpeng Wang[1]*

Corresponding authors: Qixin Zhou, qzhou@uakron.edu; Junpeng Wang, jwang6@uakron.edu

# Table of Contents

# Table of Figures and Tables

**Table S3.** Equilibrium pair potential distances ($q_{pp}$), distances between terminal carbons ($q^{\ddagger}$) and corresponding forces ($F$) for the first transition state of the two-step pathway (TS1) of the force coupled retro-Diels Alder reaction of the anthracene maleimide adduct**.** Structures did not converge at forces lower than ~126 pN.

**Table S4.** Equilibrium pair potential distances ($q_{pp}$), distances between terminal carbons ($q^{\ddagger}$) and corresponding forces ($F$) for the second transition state of the two-step pathway (TS2) of the force coupled retro-Diels Alder reaction of the anthracene–maleimide adduct**.** Structures did not converge at lower forces. Structures with negative (compressive) forces were not used in calculating the $\Delta G^{\ddagger}$.

## 1. Materials

Methyl acrylate (MA) and ethyl acrylate (EA) were flushed through a basic alumina column to remove the inhibitor and stored in a freezer for future use. All other chemicals and solvents were used as received unless otherwise noted. The anthracene–maleimide Diels–Alder adduct diacrylate (AM) was synthesized according to a previously reported procedure.[1]

## 2. Synthesis of AM-SN

The crosslinker AM (1 equiv) and photoinitiator Irgacure 819 (0.1 equiv) were dissolved in MA (100 equiv) and chloroform (50 vol%). The solution was then thoroughly deoxygenated by purging nitrogen for 15 min before being transferred via a syringe under nitrogen protection to a PTFE mold ($20\times50\times2$ $mm^3$). After UV irradiation (wavelength = 365 nm) for 1 h, the cured samples were extracted from the mold and submerged in toluene to remove any sol fraction. The solvent was decanted and replaced with fresh one for three times over the course of 24 h. The washed samples were then deswollen in methanol, dried in air and then on high vacuum at 50 °C. These samples are denoted as single networks, or AM-SN.

## 3. Synthesis of AM-DN

One SN sample at a time was allowed to swell for 24 h to equilibrium in a rubber septum capped scintillation vial (Chemglass CG-4904-01) containing a deoxygenated second monomer solution bath consisting of ethyl arylate (100 equiv), butanediol diacrylate (0.01% equiv) and Irgacure 819 (0.002% equiv). With a strong nitrogen stream input, the extra solution was carefully drawn out of the vial using a syringe with a needle. The vial was then irradiated by UV (wavelength = 365 nm) for 12 h. The cured samples were washed with methanol and dried in vacuum at 50 °C.

## 4. Tensile Testing

Uniaxial tensile testing (ASTM D1708-18) was performed on an Instron 5543 universal testing machine using pneumatic grips with a gripping pressure of 25 psi and a 100 N load cell at

a strain rate of 0.5 $min^{-1}$. Dumbbell specimens were prepared from cutting films with an ASTM D638 Type V cutting die.

## 5. Compression Experiments

Compression experiments were conducted on an Instron universal testing machine using a 50 kN load cell. The samples were cut into rectangular pieces (5x3 $mm^2$) using a fresh razor blade and a rubber mallet. Each sample was lubricated with DI water on the surface, placed between stainless steel, and compressed at a preset strain rate and $H_0/H$ ratio. The compression was held for 600 s unless specified otherwise. For systematic studies, the $H_0/H$ ratio increased from 2 to 64 in factors of 2, the strain rate ranged from 0.5 to 312.5 $min^{-1}$ in increments of 5, and the duration varied from 1 to 600 s. Each parameter was tested in triplicate. Compressive strain is defined as $(H_0-H)/H_0$, where $H_0$ and $H$ are the initial and current height, respectively.

## 6. Solid-State Fluorescence Spectroscopy

Compressed or stretched samples were measured on an Agilent Cary Eclipse fluorescence spectrometer with a solid-state sample mounter. The excitation wavelength $\lambda_{ex}$ = 365 nm and the scanned emission wavelength ranged from 380 to 500 nm. The peak intensity at wavelength 414 nm was used for calculations. The excitation and emission slit widths were both set to 2.5 nm.

## 7. Mechanochemical Activation Calibration

Radical copolymerization of MA, EA (20/80 v/v), and butanediol diacrylate (1 mol%) was initiated by V-70 (2,2'-azobis(4-methoxy-2.4-dimethyl valeronitrile)) at 35 °C in the presence of predetermined amounts of 9-anthracenemethanol (5, 10, or 15 mM) in a scintillation vial. The fluorescence intensity of the resulting films was measured by fluorescence spectroscopy. A calibration curve was established as $y = kx$, where $y$ presents fluorescence intensity and $x$ is the concentration (Fig. S1). The concentration of AM in AM-DN was calculated to be 28 mM, and the percentage of activated mechanophores after compression was obtained using the following expression: Activation (%) = $(I/k)/28\times100$, where $I$ is the fluorescence intensity of the compressed sample and $k$, the fitted slope from the calibration curve, is 85.6.

## 8. Calculating Force Coupled Ground States and Transition States

All calculations were performed using the B3LYP hybrid functional and 6-31G(d) basis set, as implemented in Gaussian 16.[2] A harmonic pair potential was applied to terminal carbons, *C1* and *C2*, of the anthracene–maleimide (AM) adduct to simulate force. This potential is given by $k(q_{pp} - q)^2$, such that the force $F = 2k(q_{pp} - q)$. Here, *k* is the force constant, $q_{pp}$ is the equilibrium pair potential distance, and q is the distance between the terminal carbons of the optimized structure. The pair potential was included using the iop(1/164=1) routine. The pair potential coupled transition states (TS) and ground states (GS) were optimized with increasing values of the equilibrium pair potential $q_{pp}$ while keeping the force constant *k* at a constant value of 0.0002 Ha/Bohr$^2$, this allowed the application of linearly increasing greater force. Optimizations were carried out using the Berny algorithm. As observed in Boulatov and co-workers' prior work (*40*), two competing pathways were identified: a concerted and a stepwise pathway. It should be noted that structure optimization was feasible only within specific force ranges for each pathway. For the concerted transition state (TSc), optimized geometries were obtained at forces between 0 and 641.1 pN, while for the two-step transition states (TS1 and TS2), they were obtained within force ranges of 126.2–2338.7 pN and -29.8–2177.9 pN, respectively. For the ground state, optimized geometries were achieved within a force range of 0–2383.0 pN. The different values of $q_{pp}$ used, the values of *q* corresponding to the optimized structures, and the resulting forces *F* for all the transition states and ground states are provided in Tables S1-4.

## 9. Calculating The Force Coupled Free Energy Barriers [$\Delta G^{\ddagger}(F)$].

The activation barriers of the force-coupled retro-Diels–Alder reaction of the AM adduct were calculated using an approach similar to the tilted potential energy surface framework (described by Marx and Ribas-Arino in their review on computational approaches in mechanochemistry[3]). To obtain the activation barriers, the reduction in the free energy barrier under force was modeled as "work" done in going from the ground state to the transition state under force *F*. This gives the following expression for $\Delta G^{\ddagger}$(F):

$$\Delta G^{\ddagger}(F) = \Delta G^{\ddagger}(F_0) - W(F) = \Delta G^{\ddagger}(F_0) - \int_{F_0}^{F} \Delta x^{\ddagger}(F)dF$$

Where $\Delta G^{\ddagger}(F)$ and $\Delta G^{\ddagger}(F_0)$ are the free energy barrier at force $F$ and some reference force $F_0$, respectively, $W(F)$ is the mechanical work done by force $F$, $\Delta x^{\ddagger}(F)$ is the change in the coordinate to which force ($F$) is applied from the GS to the TS [$q(F)^{\ddagger}$ - $q(F)$] (here, the double dagger symbol $^{\ddagger}$ denotes transition state).

The values of $q(F)$ and $q(F)^{\ddagger}$ for a range of forces were obtained from the calculations described above. To derive $\Delta x^{\ddagger}(F)$, it is essential that $q(F)$ and $q(F)^{\ddagger}$ are available for the same forces. Accordingly, the $q$ vs. $F$ data from the DFT calculations of the ground state and the various transition states (including TSc, TS1, and TS2) were fitted with an 8th-order polynomial (the data and fitting curves are shown in Fig. S10). By subtracting the fitting polynomial for $q(F)$ from $q^{\ddagger}(F)$, a function for $\Delta x^{\ddagger}(F)$ was obtained.

Subsequently, $W(F)$ was calculated for a range of force in 5 pN increments, ensuring these ranges fell within the limits for which the optimized structures of the two pathways could be calculated (0-640 pN for TSc, 130-2335 pN for TS1 and 0-2175 pN for TS2). The polynomial expression for $\Delta x^{\ddagger}(F)$ was analytically integrated, with $F_0$ as the lower limit and $F$ as the upper limit. Specifically, $F_0$ = 0 pN for the transition state of the concerted pathway (TSc) and the second step of the two-step pathway (TS2) while $F_0$ = 130 pN for the first step of the two-step pathway, as TS1 could not be optimized for forces below ~126.2 pN.

$\Delta G^{\ddagger}(F_0)$ was obtained from the DFT calculations as the sum of electronic and thermal free energy along with zero-point corrections. For TSc and TS2, this corresponded to $\Delta G^{\ddagger}(F_0)$ at 0 force (35.3 and 46.2 kcal mol$^{-1}$ respectively), while for TS1 it was at ~126.2 pN (40.4 kcal mol$^{-1}$). $\Delta G^{\ddagger}(F)$ was then obtained as indicated in the preceding equation, yielding the free energy barriers for the two pathways (Fig. S11). The concerted pathway is dominant below ~485 pN, beyond which the two-step pathway took precedence, with the first step being the rate-determining step. The force-coupled energies barriers $\Delta G^{\ddagger}(F)$ for the pathways were combined to give a single $\Delta G^{\ddagger}(F)$ vs $F$ curve (Fig. 4B in the main text). The corresponding rate constants were also calculated, using the Eyring equation:

$$k(F) = \kappa \frac{k_b T}{h} e^{\left[\frac{-\Delta G^{\ddagger}(F)}{RT}\right]}$$

Where $k$(F) is the rate constant at force $F$, $\kappa$ is the transmission coefficient (assumed to be 1), $k_b$ is the Boltzmann constant, $h$ is Planck constant, $T$ is the temperature ($T$ = 293.15 K), and $R$ is the universal gas constant.

**10. Supplementary Figures**

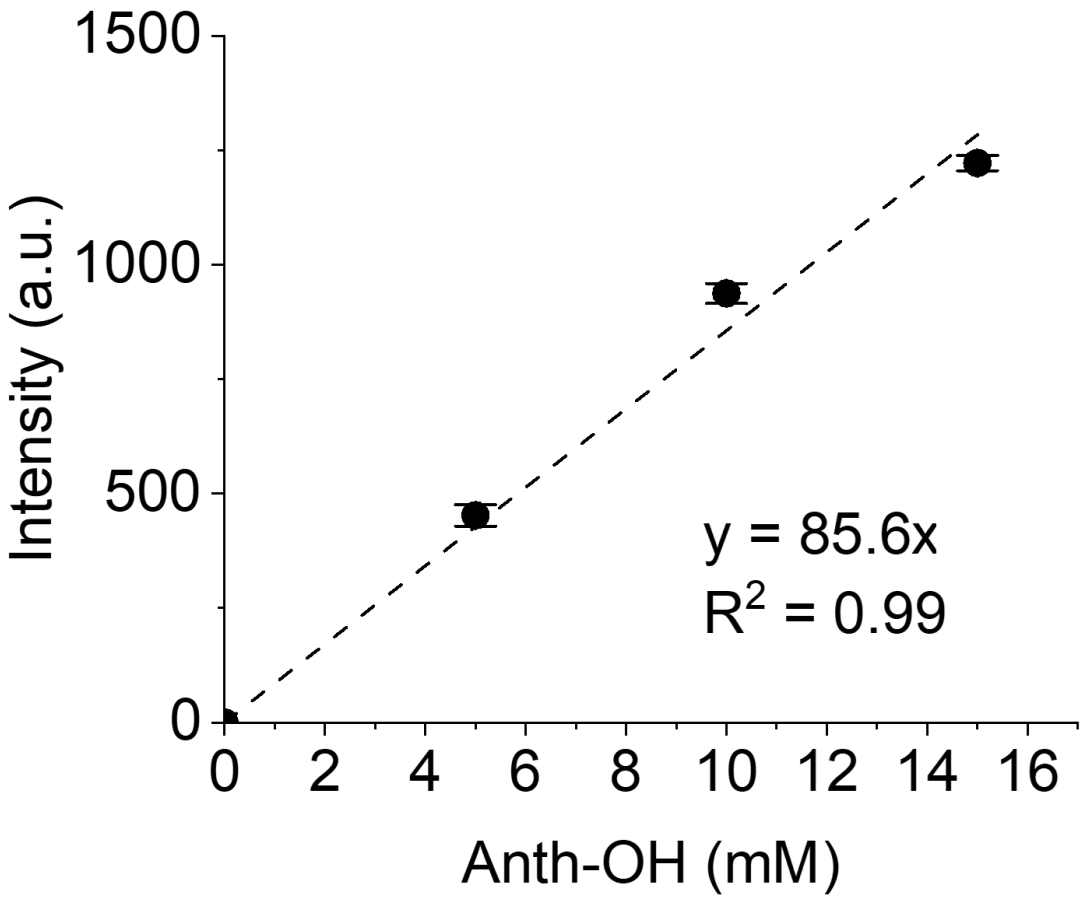


**Figure S1.** Calibration curve for mechanochemical activation, depicting the linear relationship between fluorescence intensity and anthracene concentration in MA/EA copolymer network.

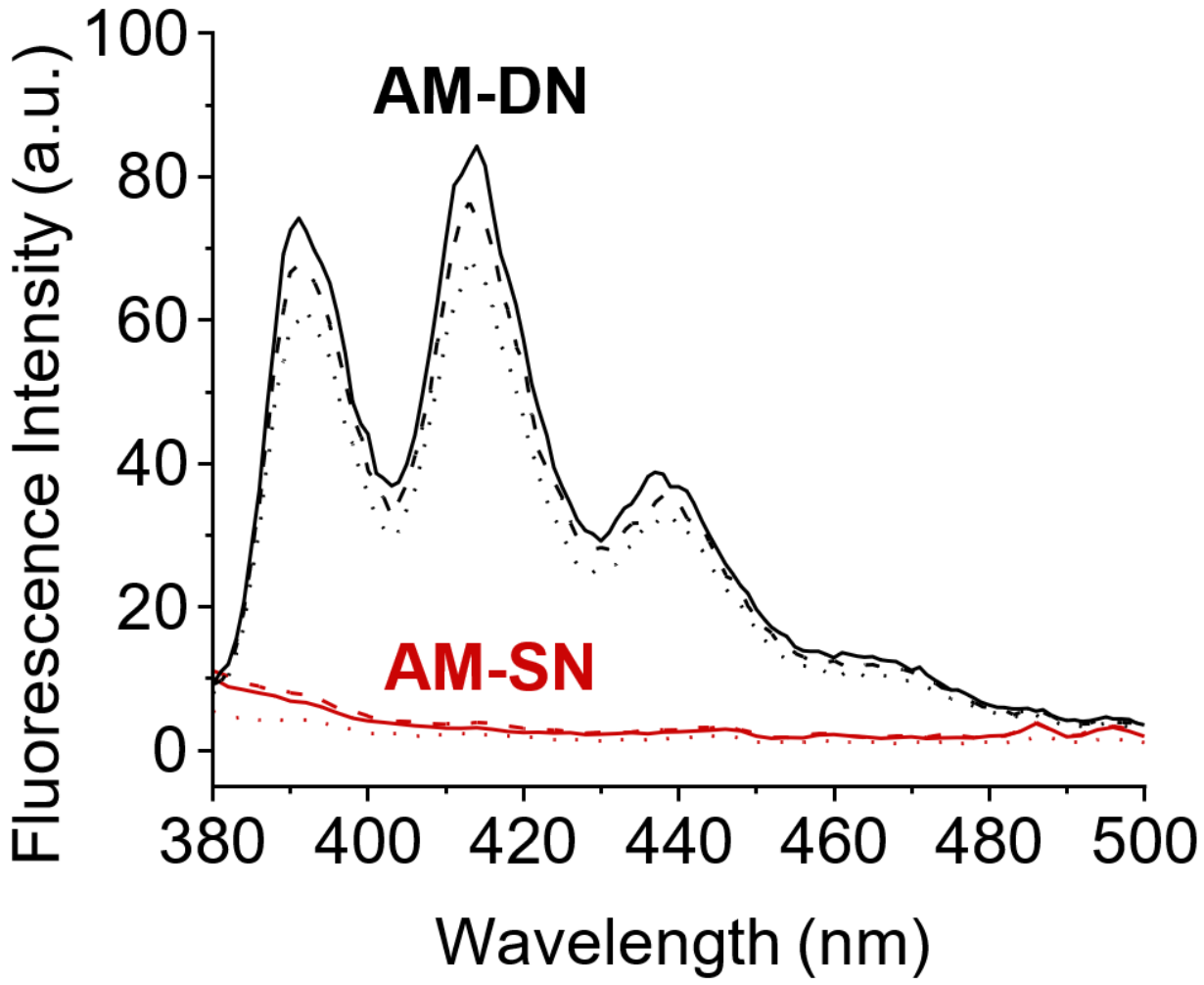


**Figure S2.** Fluorescence spectra of AM-SN (red) and AM-DN (black) in triplicate, under compression to $H_0/H = 64$ at a strain rate of 0.5 $min^{-1}$.

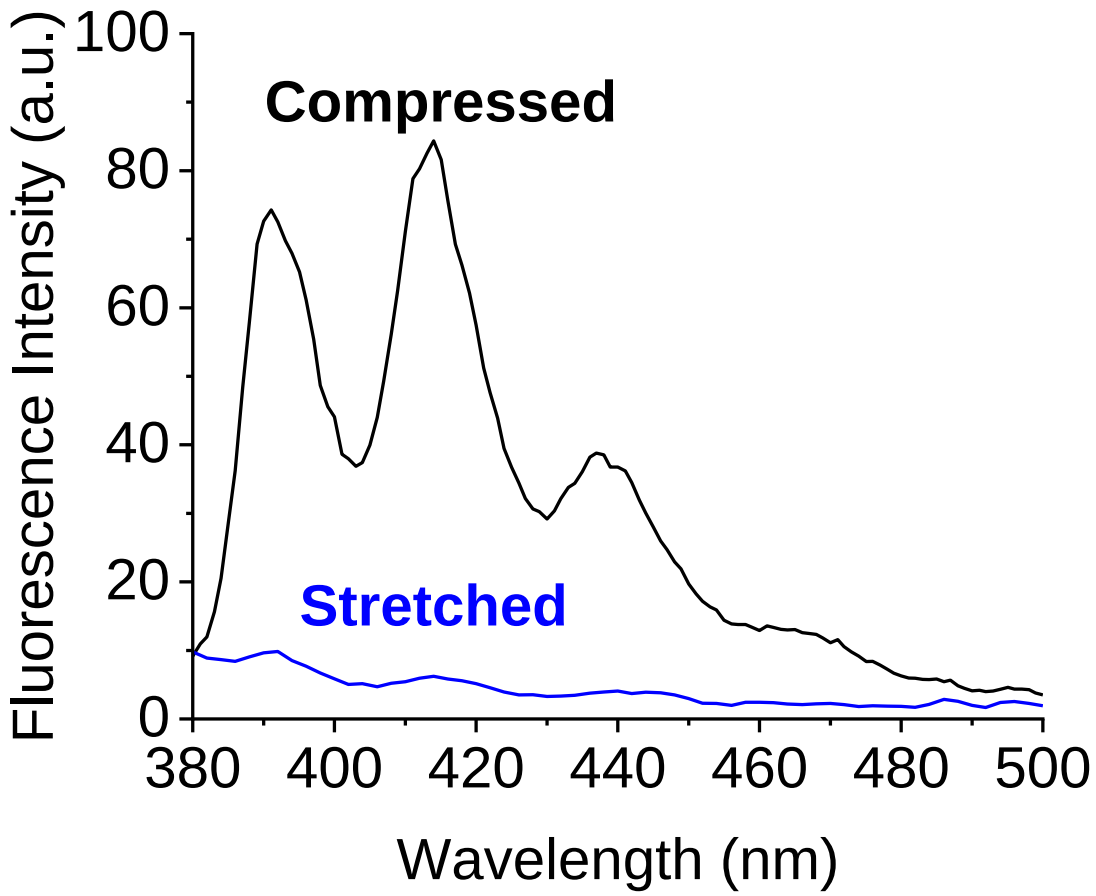


**Figure S3.** Fluorescence spectra of AM-DN samples that were compressed (black) and stretched to fracture (blue).

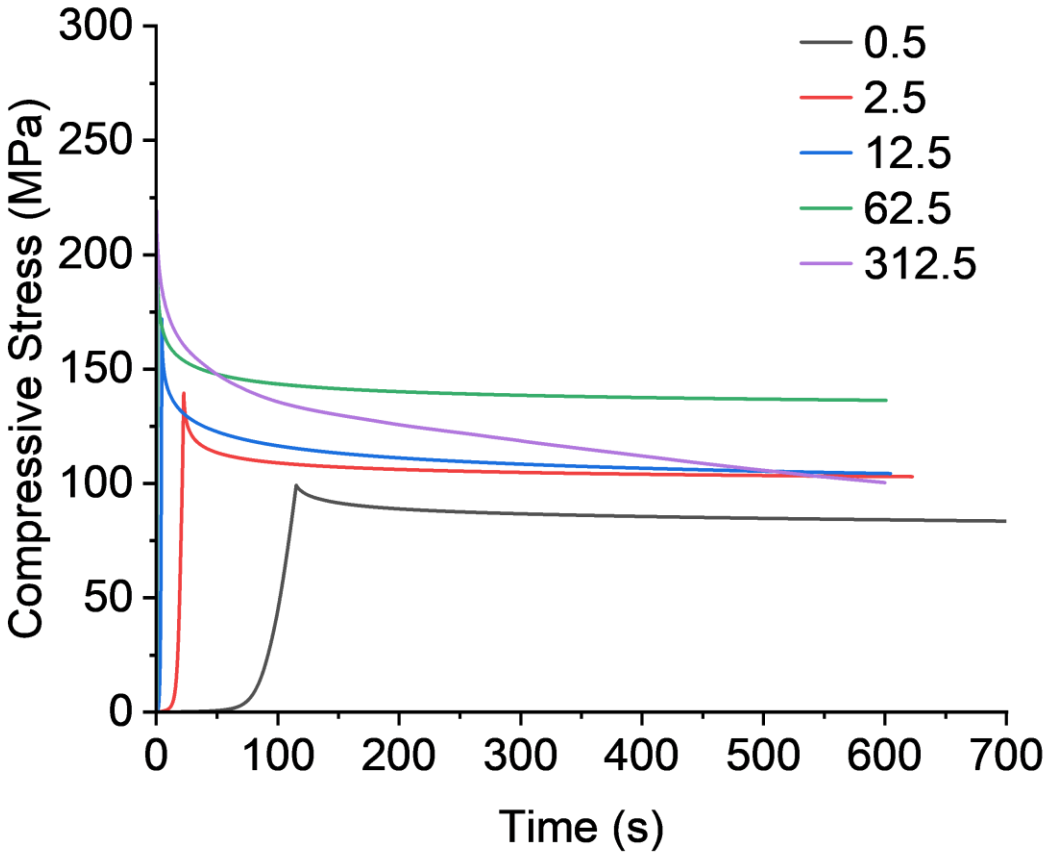


**Figure S4.** Representative stress relaxation profiles of AM-DN samples that were compressed to $H_0/H$ = 16/1 at varying strain rates. The legends in the graph represent the strain rate in $min^{-1}$.

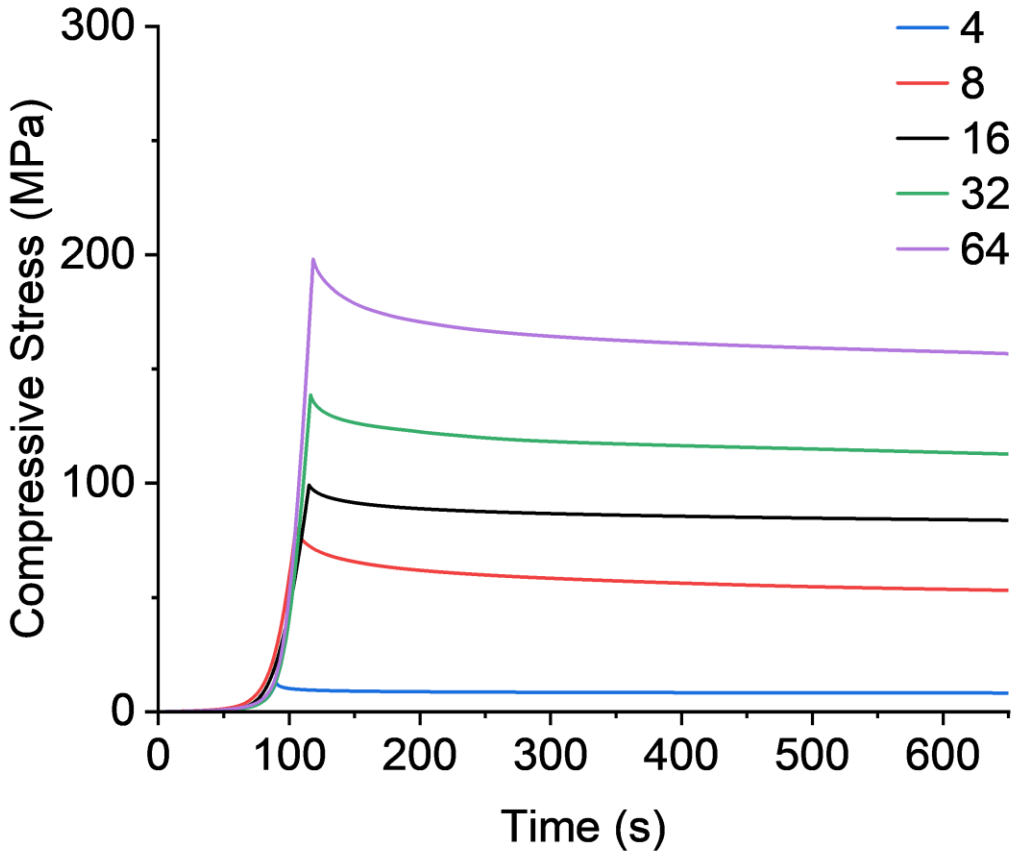


**Figure S5.** Representative stress relaxation profiles of AM-DN samples that were compressed to various $H_0/H$ ratios (indicated by the numbers in the figure) at a strain rate of 0.5 $min^{-1}$. The legends in the graph represent the $H_0/H$.

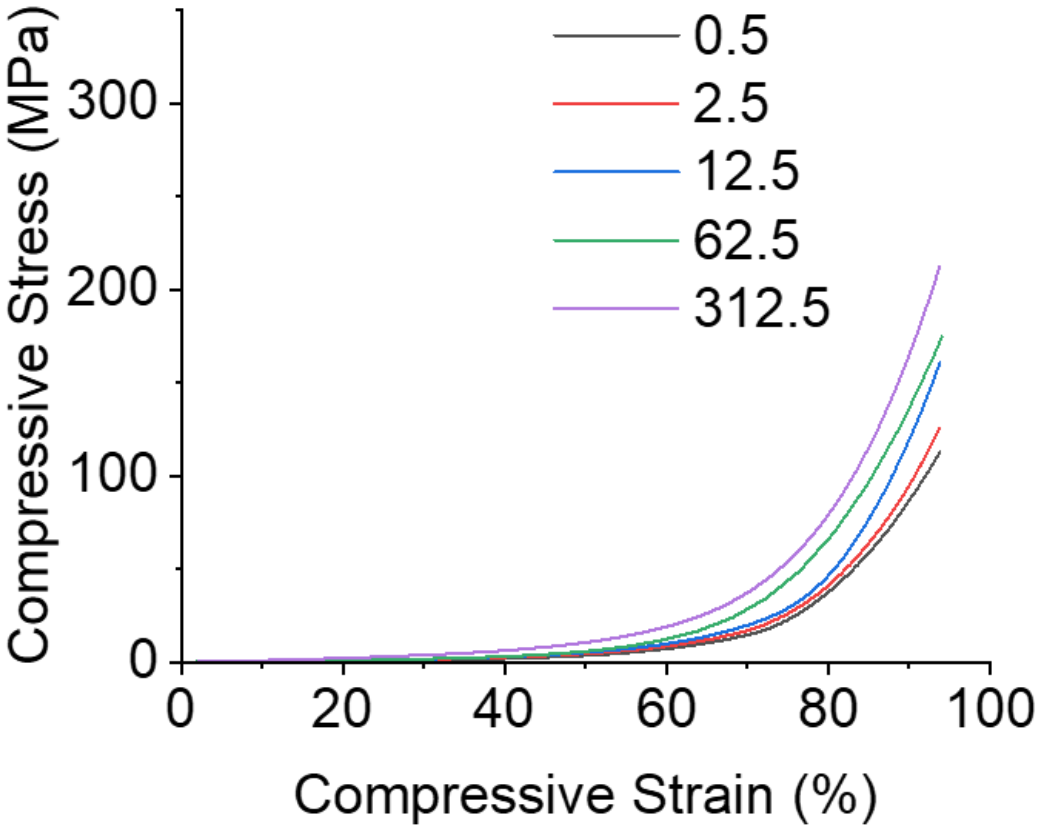


**Figure S6.** Representative stress-strain curves of AM-DN samples that were compressed to $H_0/H$ = 16 at varying strain rates ranging from 0.5 to 312.5 $min^{-1}$. The legends in the graphs indicate the strain rates in $min^{-1}$.

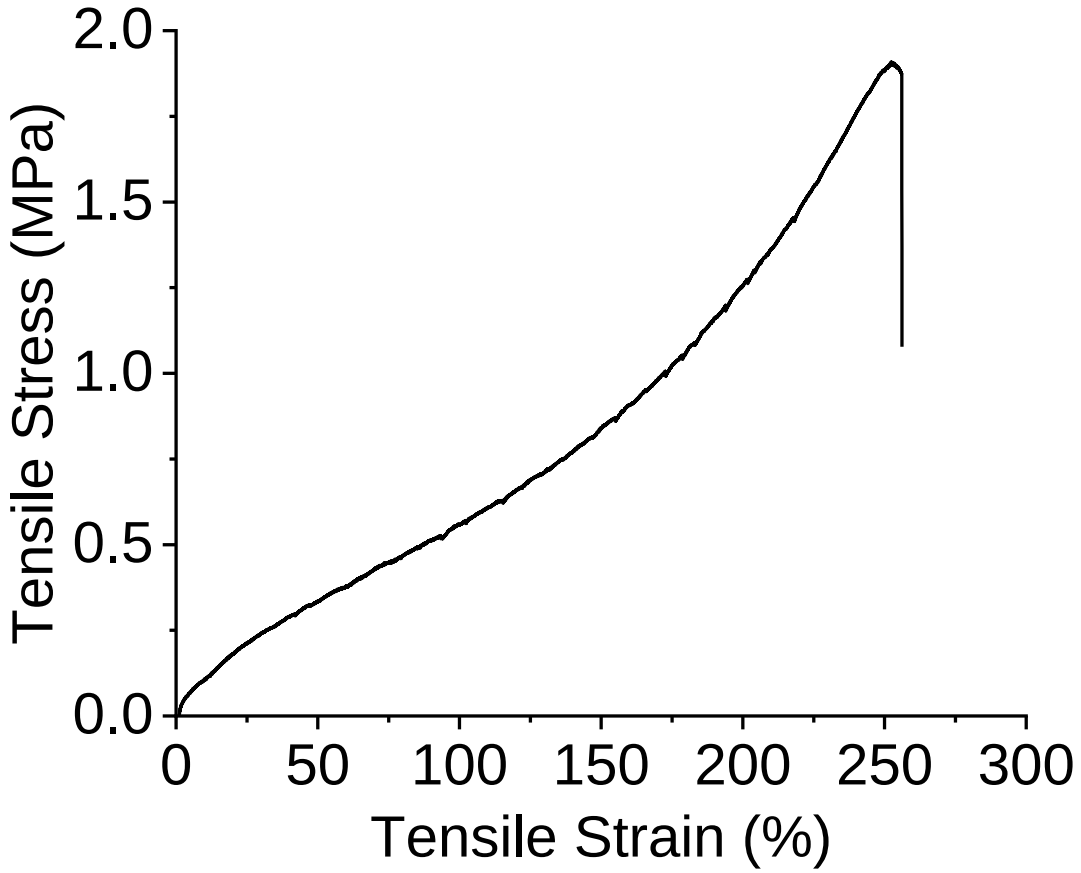


**Figure S7.** Representative stress-strain curve of an AM-DN dumbbell sample that was uniaxially stretched to failure at a strain rate of 0.5 $min^{-1}$.

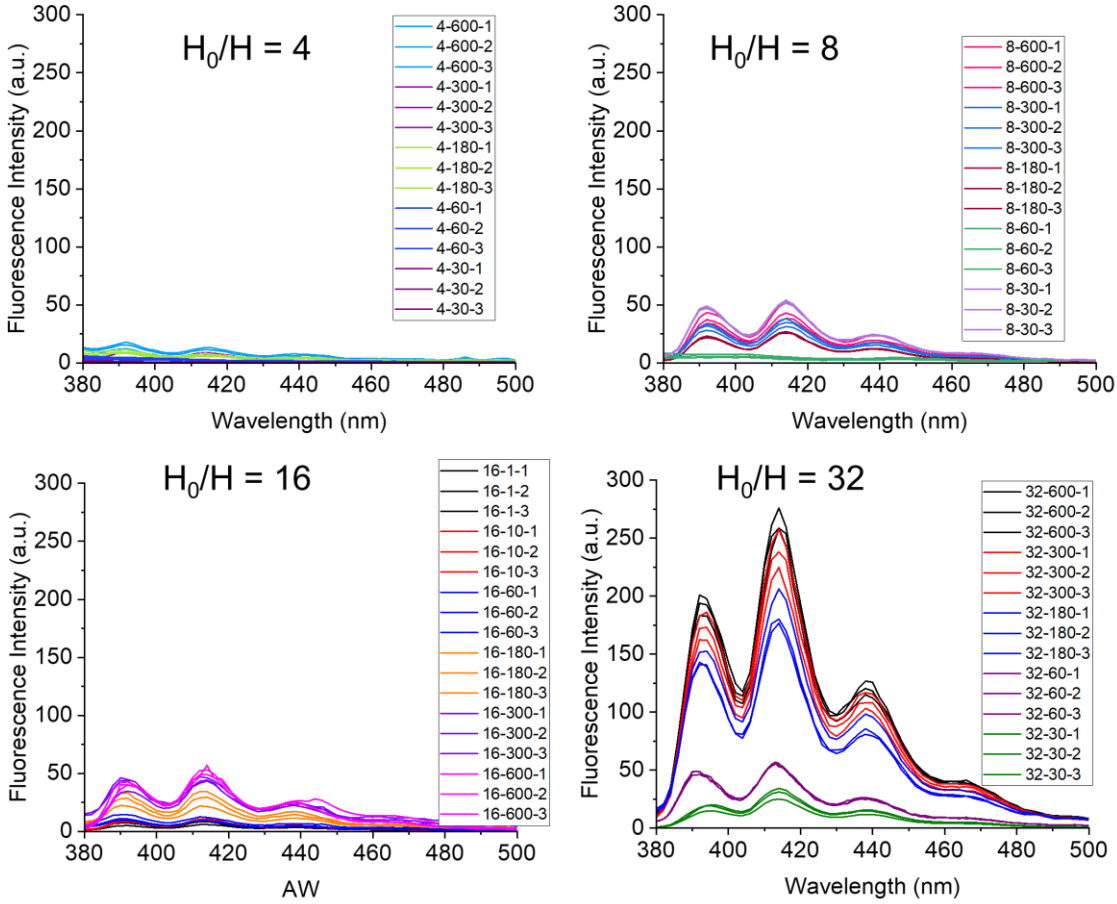


**Figure S8.** Fluorescence spectra of AM-DN samples that had been compressed to various compression ratios $H_0/H$ at a strain rate of 0.5 $min^{-1}$ and held for various durations of time. Each condition was conducted in triplicates. In the legends, the first number indicates the compression ratio $H_0/H$, the second number represents the isometric hold duration, and the third number denotes the sample entry. For example, 4-600-2 refers to the second sample in a triplicate that was compressed to $H_0/H = 4$ at a strain rate of 0.5 $min^{-1}$ and held for 600 s.

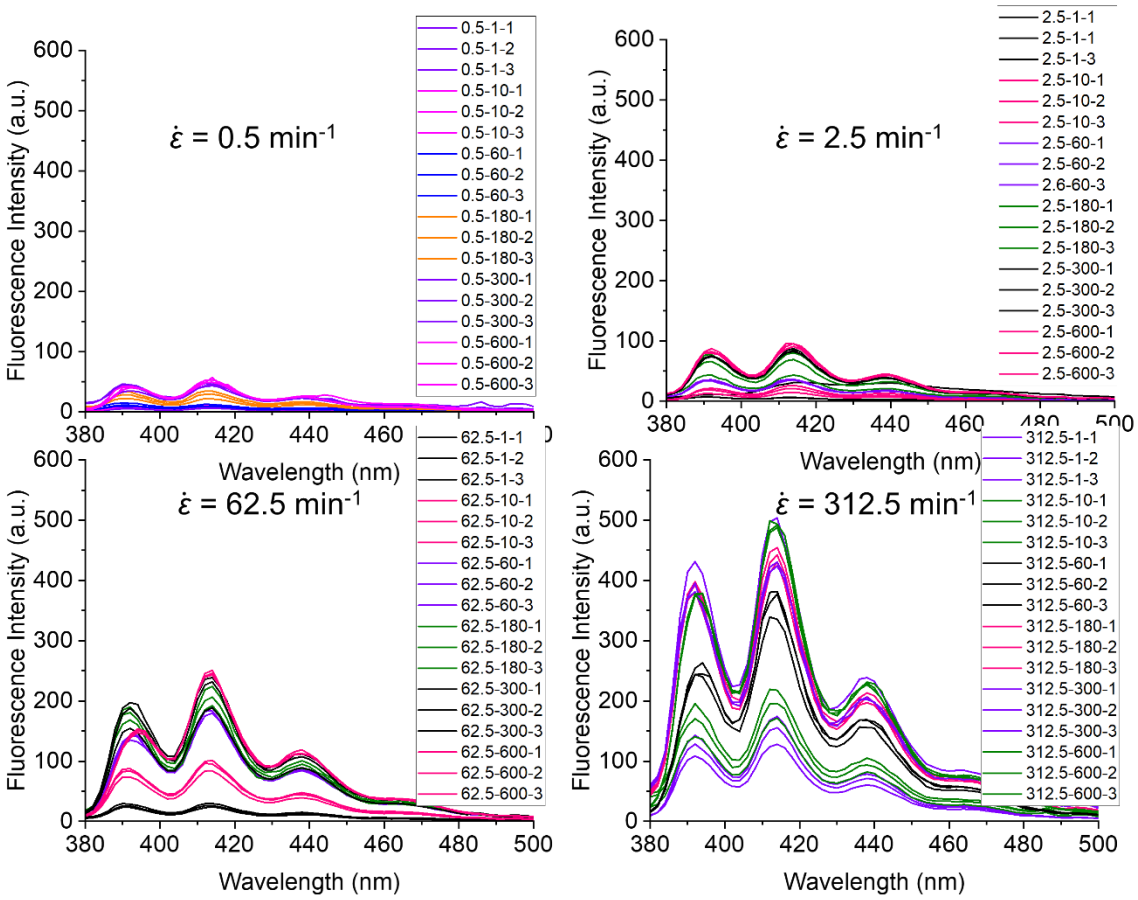


**Figure S9.** Fluorescence spectra of AM-DN samples that had been compressed to $H_0/H$ = 16 at various strain rates and held for various durations of time. Each condition was conducted in triplicates. In the legends, the first number indicates the strain rate, the second number represents isometric hold duration, and the third number denotes the sample entry. For example, 0.5-1-3 refers to the third sample in a triplicate that was compressed to $H_0/H$ = 16 at a strain rate of 0.5 min$^{-1}$ and held for 1 s.

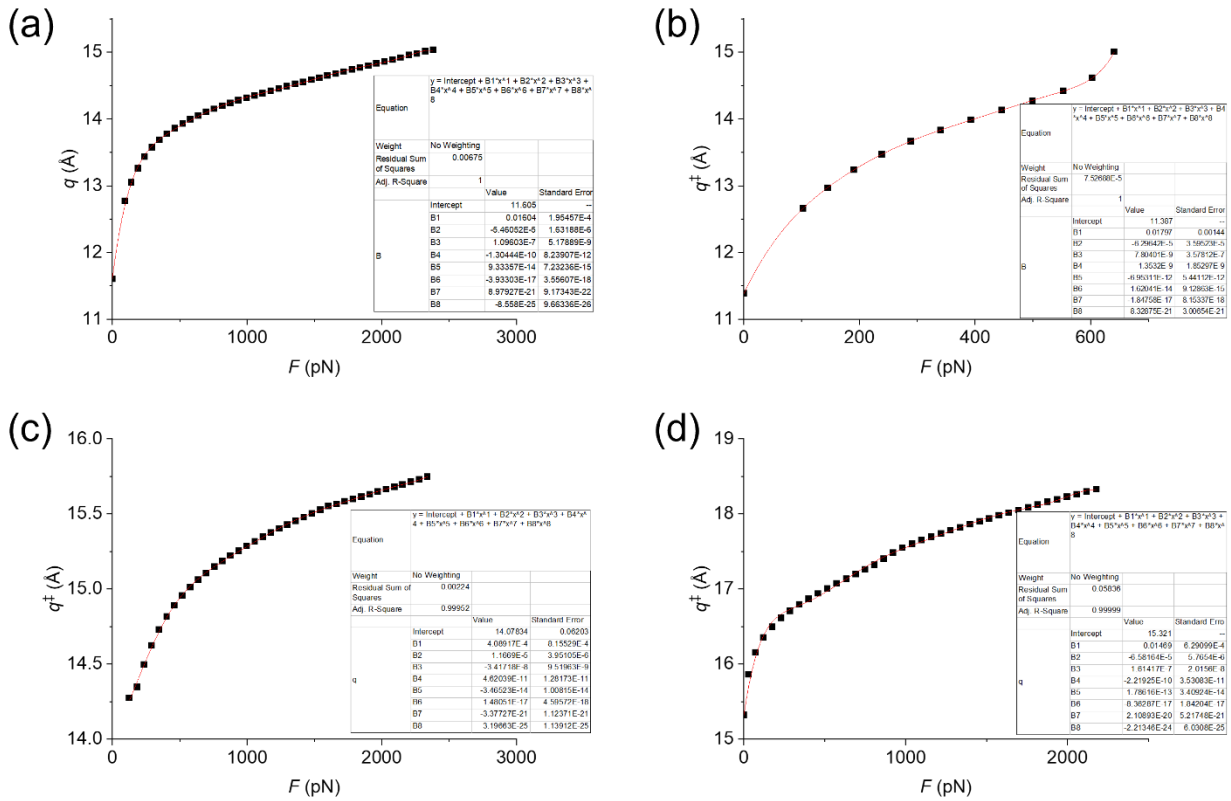


**Figure S10.** $q$ and $q^{\ddagger}$ vs $F$ curves and their corresponding fitted polynomials for (a) the ground state GS, (b) the concerted transition state (TSc), and transition state for (c) step 1 (TS1) and (d) step 2 (TS2) of the two-step pathway in the force-induced retro-Diels–Alder reaction of the anthracene–maleimide adduct.

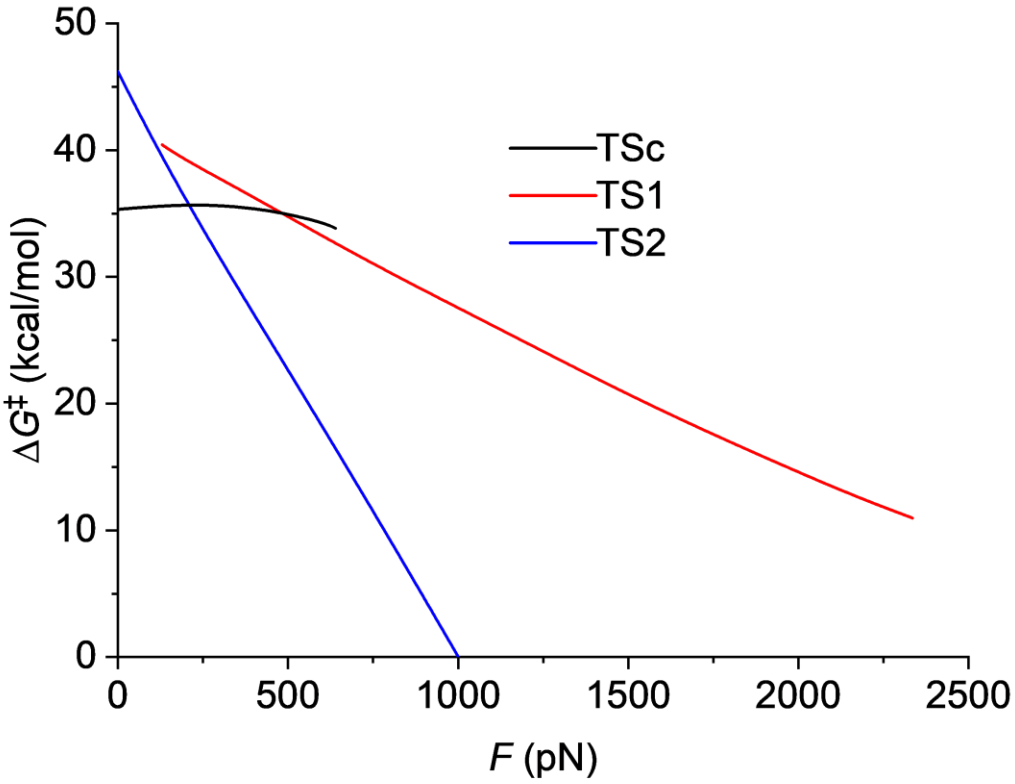


**Figure S11.** Free energy barriers for the concerted (TSc) and two-step (TS1 and TS2) pathways in the force-coupled retro-Diels–Alder reaction of anthracene–maleimide.

## 11. Supplementary Tables

**Table S1.** Equilibrium pair potential distances (qpp), distances between terminal carbons (q) and corresponding forces (F) for the reactant ground state (GS) of the force coupled retro-Diels Alder reaction of the anthracene–maleimide adduct.

| Sr. No. | $q_{pp}$ (Å) | F (pN) | q (Å) |
|---|---|---|---|
| 0 | - | 0.000 | 11.605 |
| 1 | 14.3 | 95.225 | 12.771 |
| 2 | 15.3 | 140.253 | 13.048 |
| 3 | 16.3 | 189.204 | 13.262 |
| 4 | 17.3 | 240.646 | 13.436 |
| 5 | 18.3 | 294.393 | 13.573 |
| 6 | 19.3 | 349.696 | 13.685 |
| 7 | 20.3 | 406.121 | 13.779 |
| 8 | 21.3 | 463.355 | 13.86 |
| 9 | 22.3 | 521.212 | 13.931 |
| 10 | 23.3 | 579.567 | 13.994 |
| 11 | 24.3 | 638.358 | 14.05 |
| 12 | 25.3 | 697.398 | 14.102 |
| 13 | 26.3 | 756.687 | 14.15 |
| 14 | 27.3 | 816.226 | 14.194 |
| 15 | 28.3 | 875.889 | 14.236 |
| 16 | 29.3 | 935.676 | 14.276 |
| 17 | 30.3 | 995.526 | 14.315 |
| 18 | 31.3 | 1055.500 | 14.352 |
| 19 | 32.3 | 1115.599 | 14.387 |
| 20 | 33.3 | 1175.698 | 14.422 |
| 21 | 34.3 | 1235.859 | 14.456 |
| 22 | 35.3 | 1296.083 | 14.489 |
| 23 | 36.3 | 1356.306 | 14.522 |
| 24 | 37.3 | 1416.592 | 14.554 |
| 25 | 38.3 | 1476.940 | 14.585 |

| | | | |
|---|---|---|---|
| 26 | 39.3 | 1537.226 | 14.617 |
| 27 | 40.3 | 1597.574 | 14.648 |
| 28 | 41.3 | 1657.984 | 14.678 |
| 29 | 42.3 | 1718.332 | 14.709 |
| 30 | 43.3 | 1778.742 | 14.739 |
| 31 | 44.3 | 1839.153 | 14.769 |
| 32 | 45.3 | 1899.563 | 14.799 |
| 33 | 46.3 | 1959.973 | 14.829 |
| 34 | 47.3 | 2020.383 | 14.859 |
| 35 | 48.3 | 2080.794 | 14.889 |
| 36 | 49.3 | 2141.204 | 14.919 |
| 37 | 50.3 | 2201.054 | 14.958 |
| 38 | 51.3 | 2262.087 | 14.978 |
| 39 | 52.3 | 2322.435 | 15.009 |
| 40 | 53.3 | 2383.032 | 15.036 |

**Table S2.** Equilibrium pair potential distances ($q_{pp}$), distances between terminal carbons ($q^{\ddagger}$) and corresponding forces ($F$) for the concerted transition state (TSc) of the force coupled retro-Diels Alder reaction of the anthracene maleimide adduct.

| Sr. No. | $q_{pp}$ (Å) | F (pN) | q (Å) |
|---|---|---|---|
| 0 | 0 | 0.000 | 11.387 |
| 1 | 14.3 | 102.075 | 12.661 |
| 2 | 15.3 | 145.109 | 12.970 |
| 3 | 16.3 | 190.510 | 13.241 |
| 4 | 17.3 | 238.527 | 13.47 |
| 5 | 18.3 | 288.723 | 13.664 |
| 6 | 19.3 | 340.477 | 13.833 |
| 7 | 20.3 | 393.165 | 13.987 |
| 8 | 21.3 | 446.413 | 14.132 |
| 9 | 22.3 | 499.785 | 14.275 |
| 10 | 23.3 | 552.971 | 14.421 |
| 11 | 24.3 | 603.230 | 14.614 |
| 12 | 25.3 | 641.095 | 15.006 |

**Table S3.** Equilibrium pair potential distances ($q_{pp}$), distances between terminal carbons ($q^{\ddagger}$) and corresponding forces ($F$) for the first transition state of the two-step pathway (TS1) of the force coupled retro-Diels Alder reaction of the anthracene maleimide adduct**.** Structures did not converge at forces lower than ~126 pN.

| Sr. No. | $q_{pp}$ (Å) | F (pN) | q (Å) |
|---|---|---|---|
| 1 | 16.3 | 126.176 | 14.274 |
| 2 | 17.3 | 183.846 | 14.348 |
| 3 | 18.3 | 236.845 | 14.497 |
| 4 | 19.3 | 291.152 | 14.625 |
| 5 | 20.3 | 346.954 | 14.729 |
| 6 | 21.3 | 403.752 | 14.817 |
| 7 | 22.3 | 461.360 | 14.892 |
| 8 | 23.3 | 519.652 | 14.956 |
| 9 | 24.3 | 578.443 | 15.012 |
| 10 | 25.3 | 637.608 | 15.062 |
| 11 | 26.3 | 697.084 | 15.107 |
| 12 | 27.3 | 756.809 | 15.148 |
| 13 | 28.3 | 816.721 | 15.186 |
| 14 | 29.3 | 876.758 | 15.222 |
| 15 | 30.3 | 936.981 | 15.255 |
| 16 | 31.3 | 997.267 | 15.287 |
| 17 | 32.3 | 1057.614 | 15.318 |
| 18 | 33.3 | 1118.087 | 15.347 |
| 19 | 34.3 | 1178.622 | 15.375 |
| 20 | 35.3 | 1239.219 | 15.402 |
| 21 | 36.3 | 1299.878 | 15.428 |
| 22 | 37.3 | 1360.537 | 15.454 |
| 23 | 38.3 | 1421.259 | 15.479 |
| 24 | 39.3 | 1481.981 | 15.504 |
| 25 | 40.3 | 1542.702 | 15.529 |
| 26 | 41.3 | 1603.548 | 15.552 |
| 27 | 42.3 | 1664.893 | 15.567 |

| | | | |
|---|---|---|---|
| 28 | 43.3 | 1726.175 | 15.583 |
| 29 | 44.3 | 1787.457 | 15.599 |
| 30 | 45.3 | 1848.739 | 15.615 |
| 31 | 46.3 | 1910.021 | 15.631 |
| 32 | 47.3 | 1971.241 | 15.648 |
| 33 | 48.3 | 2032.523 | 15.664 |
| 34 | 49.3 | 2093.743 | 15.681 |
| 35 | 50.3 | 2155.025 | 15.697 |
| 36 | 51.3 | 2216.245 | 15.714 |
| 37 | 52.3 | 2277.527 | 15.73 |
| 38 | 53.3 | 2338.747 | 15.747 |

**Table S4.** Equilibrium pair potential distances ($q_{pp}$), distances between terminal carbons ($q^{\ddagger}$) and corresponding forces ($F$) for the second transition state of the two-step pathway (TS2) of the force coupled retro-Diels Alder reaction of the anthracene–maleimide adduct**.** Structures did not converge at lower forces. Structures with negative (compressive) forces were not used in calculating the $\Delta G^{\ddagger}$.

| Sr. No. | $q_{pp}$ (Å) | F (pN) | q (Å) |
|---|---|---|---|
| 0 | - | 0.000 | 15.321 |
| 1 | 14.3 | -29.769 | 14.778 |
| 2 | 15.3 | -0.623 | 15.310 |
| 3 | 16.3 | 27.278 | 15.862 |
| 4 | 17.3 | 71.496 | 16.152 |
| 5 | 18.3 | 121.443 | 16.35 |
| 6 | 19.3 | 174.629 | 16.496 |
| 7 | 20.3 | 229.683 | 16.612 |
| 8 | 21.3 | 285.983 | 16.708 |
| 9 | 22.3 | 342.968 | 16.793 |
| 10 | 23.3 | 400.513 | 16.869 |
| 11 | 24.3 | 458.308 | 16.941 |
| 12 | 25.3 | 516.414 | 17.008 |
| 13 | 26.3 | 574.707 | 17.072 |
| 14 | 27.3 | 632.999 | 17.136 |
| 15 | 28.3 | 691.417 | 17.198 |
| 16 | 29.3 | 749.834 | 17.26 |
| 17 | 30.3 | 808.064 | 17.325 |
| 18 | 31.3 | 865.610 | 17.401 |
| 19 | 32.3 | 922.595 | 17.486 |
| 20 | 33.3 | 980.887 | 17.55 |
| 21 | 34.3 | 1039.927 | 17.602 |
| 22 | 35.3 | 1099.279 | 17.649 |
| 23 | 36.3 | 1158.693 | 17.695 |
| 24 | 37.3 | 1218.293 | 17.738 |
| 25 | 38.3 | 1277.956 | 17.78 |

| | | | |
|---|---|---|---|
| 26 | 39.3 | 1337.681 | 17.821 |
| 27 | 40.3 | 1397.406 | 17.862 |
| 28 | 41.3 | 1457.194 | 17.902 |
| 29 | 42.3 | 1517.043 | 17.941 |
| 30 | 43.3 | 1576.955 | 17.979 |
| 31 | 44.3 | 1636.930 | 18.016 |
| 32 | 45.3 | 1696.904 | 18.053 |
| 33 | 46.3 | 1757.003 | 18.088 |
| 34 | 47.3 | 1817.039 | 18.124 |
| 35 | 48.3 | 1877.138 | 18.159 |
| 36 | 49.3 | 1937.237 | 18.194 |
| 37 | 50.3 | 1997.398 | 18.228 |
| 38 | 51.3 | 2057.559 | 18.262 |
| 39 | 52.3 | 2117.782 | 18.295 |
| 40 | 53.3 | 2177.943 | 18.329 |

## 12. References


1. Kabb, C. P.; O'Bryan, C. S.; Morley, C. D.; Angelini, T. E.; Sumerlin, B. S., Anthracene-Based Mechanophores for Compression-Activated Fluorescence in Polymeric Networks. *Chem. Sci.* **2019,** *10* (33), 7702-7708.

2. Frisch, M. J.; Trucks, G. W.; Schlegel, H. B.; Scuseria, G. E.; Robb, M. A.; Cheeseman, J. R.; Scalmani, G.; Barone, V.; Petersson, G. A.; Nakatsuji, H.; Li, X.; Caricato, M.; Marenich, A. V.; Bloino, J.; Janesko, B. G.; Gomperts, R.; Mennucci, B.; Hratchian, H. P.; Ortiz, J. V.; Izmaylov, A. F.; Sonnenberg, J. L.; Williams; Ding, F.; Lipparini, F.; Egidi, F.; Goings, J.; Peng, B.; Petrone, A.; Henderson, T.; Ranasinghe, D.; Zakrzewski, V. G.; Gao, J.; Rega, N.; Zheng, G.; Liang, W.; Hada, M.; Ehara, M.; Toyota, K.; Fukuda, R.; Hasegawa, J.; Ishida, M.; Nakajima, T.; Honda, Y.; Kitao, O.; Nakai, H.; Vreven, T.; Throssell, K.; Montgomery Jr., J. A.; Peralta, J. E.; Ogliaro, F.; Bearpark, M. J.; Heyd, J. J.; Brothers, E. N.; Kudin, K. N.; Staroverov, V. N.; Keith, T. A.; Kobayashi, R.; Normand, J.; Raghavachari, K.; Rendell, A. P.; Burant, J. C.; Iyengar, S. S.; Tomasi, J.; Cossi, M.; Millam, J. M.; Klene, M.; Adamo, C.; Cammi, R.; Ochterski, J. W.; Martin, R. L.; Morokuma, K.; Farkas, O.; Foresman, J. B.; Fox, D. J. *Gaussian 16 Rev. C.01*, Wallingford, CT, 2016.

3. Ribas-Arino, J.; Marx, D., Covalent Mechanochemistry: Theoretical Concepts and Computational Tools with Applications to Molecular Nanomechanics. *Chem. Rev.* **2012,** *112* (10), 5412-5487.